A magnetic and Mössbauer spectral study of $TbFe_{11}Ti$ and $TbFe_{11}TiH$

2003 J. Phys.: Condens. Matter 15 7395

(http://iopscience.iop.org/0953-8984/15/43/021)

INSTITUTE OF PHYSICS PUBLISHING JOURNAL OF PHYSICS: CONDENSED MATTER

J. Phys.: Condens. Matter **15** (2003) 7395–7409 PII: S0953-8984(03)64545-5

A magnetic and Mössbauer spectral study of $TbFe_{11}Ti$ and $TbFe_{11}TiH$

Cristina Piquer[1], Raphaël P Hermann[1], Fernande Grandjean[1], Olivier Isnard[2] and Gary J Long[3]

[1] Institut de Physique, B5, Université de Liège, B-4000 Sart-Tilman, Belgium
[2] Laboratoire de Cristallographie du CNRS, Associé à l'Université J Fourier et à l'INPG, CNRS, F-38042 Grenoble, France
[3] Department of Chemistry, University of Missouri-Rolla, Rolla, MO 65409-0010, USA

E-mail: fgrandjean@ulg.ac.be, isnard@labs.polycnrs-gre.fr and glong@umr.edu

Received 10 June 2003
Published 17 October 2003
Online at stacks.iop.org/JPhysCM/15/7395

Abstract

Magnetic and iron-57 Mössbauer spectral measurements between 4.2 and 640 K have been carried out on $TbFe_{11}Ti$ and $TbFe_{11}TiH$. The insertion of hydrogen into $TbFe_{11}Ti$ to form $TbFe_{11}TiH$ increases its ordering temperature, magnetization, magnetic hyperfine fields, and isomer shifts as a result of lattice expansion. Further, the insertion of hydrogen reinforces the basal magnetic anisotropy of the terbium sublattice and, as is shown by ac susceptibility measurements and thermomagnetic analysis, the spin reorientation observed in $TbFe_{11}Ti$ at 338 K disappears in $TbFe_{11}TiH$. The Mössbauer spectra have been analysed with a model that considers both the easy magnetization direction and the distribution of titanium atoms in the near-neighbour environment of the three crystallographically distinct iron sites. The assignment and the temperature dependencies of the hyperfine fields and isomer shifts are in complete agreement with a Wigner–Seitz cell analysis of the three iron sites in $RFe_{11}Ti$ and $RFe_{11}TiH$, where R is a rare-earth element. A complete analysis of the quadrupole interactions in both magnetic phases and in the paramagnetic phase of $TbFe_{11}Ti$ supports the Mössbauer spectral analysis, and indicates that in the basal magnetic phase the iron magnetic moments are oriented along the equivalent [100] and [010] directions of the unit cell.

1. Introduction

The series of $RFe_{12-x}M_x$ compounds, where R is a rare-earth element and M is a transition metal, has two main advantages as hard magnetic materials: first, a high iron content which yields a high magnetization and, second, a relatively high Curie temperature. These compounds crystallize with the $I4/mmm$ $ThMn_{12}$ structure [1–4], and, in general, the interstitial insertion

of light elements, such as hydrogen, carbon, or nitrogen, into the structure has a dramatic and beneficial effect upon the compound's magnetic properties [5]. Indeed, the insertion of interstitial elements into the $RFe_{11}Ti$ compounds leads to large changes in their lattice parameters and magnetic properties [6–11].

$TbFe_{11}Ti$ is reported [12–21] to exhibit a magnetic spin reorientation at temperatures between 325 and 339 K. The sensitivity of the spin-reorientation temperature to the applied magnetic field used by different authors for these measurements yields a spread in the reported temperatures [14, 20]. As has been shown by single crystal magnetization measurements [12], below this spin-reorientation temperature, i.e., below about 330 K, the terbium magnetic anisotropy dominates and the easy magnetization direction is aligned along the [100] axis in the basal plane of the tetragonal unit cell. Above about 330 K, the iron magnetic anisotropy dominates and the easy magnetization direction is along the *c*-axis of the tetragonal unit cell. The spin reorientation at about 330 K has been found to be first order by Nikitin *et al* [12, 15]. In contrast, Abadia *et al* [16] observed a temperature range for the spin reorientation from perpendicular to the *c*-axis at 280 K to parallel to the *c*-axis at 330 K. They attributed the observed intermediate easy magnetization directions to the coexistence of the two magnetic anisotropies, perpendicular and parallel to the *c*-axis, between 280 and 330 K. In addition, Nikitin *et al* [12, 15] have also concluded that the hydride of $TbFe_{11}Ti$ shows no spin reorientation and exhibits basal magnetic anisotropy at all temperatures below its Curie temperature.

Herein we report magnetic measurements and iron-57 Mössbauer spectral studies between 4.2 and 640 K on $TbFe_{11}Ti$ and between 4.2 and 295 K on $TbFe_{11}TiH$. The goal of this work is to investigate the influence of hydrogen insertion on the spin reorientation and on the Mössbauer spectral hyperfine parameters and thus on the magnetic properties of the iron sublattices.

2. Experimental details

$TbFe_{11}Ti$ has been synthesized in a water-cooled copper crucible by melting 99.95% pure terbium and titanium and 99.99% pure iron in a high frequency induction furnace. A high homogeneity was achieved by annealing the sample at 1200 K for 10 days. The hydrogen insertion was carried out at 300 K under 20 bar of hydrogen gas after a 10 min thermal activation at 580 K, an activation that initiates the insertion of the hydrogen. The hydrogen content was determined by measuring the gain in mass and is accurate to ± 0.1 hydrogen atom/fu.

X-ray diffraction patterns were recorded with a Guinier–Hägg focusing camera with 1.9373 Å iron $K_{\alpha 1}$ radiation; silicon powder was used as an internal standard. The lattice parameters have been refined from 24 observed Bragg reflections.

The thermomagnetic analyses of the samples, sealed in a silica tube under hydrogen gas in order to avoid oxidation and to minimize hydrogen loss, were performed on a Faraday balance. The isothermal magnetization curves were obtained at 5 and 300 K with the extraction method [22] in a dc field of up to 7 T. The saturation magnetization values have been derived, as discussed earlier [7], by extrapolation to zero field of the magnetization results obtained in fields above 4 T.

The low temperature ac magnetic susceptibilities were obtained on a computer controlled mutual inductance susceptometer [23] at an exciting field of 10^{-4} T and a frequency of 120 Hz. A lock-in amplifier was used to measure the complex susceptibility, $\chi_{ac} = \chi' - j\chi''$, where χ' is the initial susceptibility, a quantity which is related to the variation in the sample magnetization, and χ'' is non-zero if magnetic energy is absorbed by the sample. The temperature dependence of the real component, χ', and the imaginary component, χ'', of the ac susceptibility was measured in order to determine the temperature of the magnetic phase transitions. These

Table 1. The lattice parameters, Curie temperatures, and saturation magnetizations of $TbFe_{11}Ti$ and $TbFe_{11}TiH$.

Compound	a (Å)	c (Å)	c/a	V (Å^3)	T_C (K)	$M_s^{5\ K}$ (μ_B/fu)	$M_s^{300\ K}$ (μ_B/fu)
$TbFe_{11}Ti$	8.515(1)	4.790(1)	0.5625(2)	347.3(1)	578(5)	10.5	11.7
$TbFe_{11}TiH$	8.548(1)	4.803(1)	0.5619(2)	351.0(1)	620(5)	11.3	12.2

measurements are very sensitive to the onset of the magnetic phase transition caused by changes in the anisotropy energy. The real part of the ac susceptibility is determined predominately by the changes in both the magnetic anisotropy energy and the domain wall energy, whereas the imaginary ac susceptibility reflects energy absorption by the sample, an energy which is mainly derived from domain wall movement.

The Mössbauer spectra have been measured between 4.2 and 640 K on a constant-acceleration spectrometer which utilized a rhodium matrix cobalt-57 source and was calibrated at room temperature with α-iron foil. The Mössbauer spectral absorbers contained 35 mg cm^{-2} of powdered sample which had been sieved to a 0.045 mm or smaller diameter particle size. The low temperature spectra were measured in a Janis Super-Varitemp cryostat and the temperature was controlled with a Lakeshore Cryogenics temperature controller with an accuracy of better than 1% of the observed temperature. The high temperature spectra were obtained in a high vacuum oven and the sample temperature was measured with an FeRh thermocouple and controlled with a Thor temperature controller with an accuracy of ± 10 K. The resulting spectra have been fit as discussed below and the estimated errors are at most ± 0.2 T for the hyperfine fields and their incremental changes, ± 0.01 mm s^{-1} for the isomer shifts and their incremental changes, and ± 0.02 mm s^{-1} for the quadrupole shifts and their incremental changes. The observed line widths in the magnetic spectra were typically 0.38 ± 0.02 and 0.34 ± 0.02 mm s^{-1} for $TbFe_{11}Ti$ and $TbFe_{11}TiH$, respectively.

3. Structural and magnetic results

$TbFe_{11}Ti$ crystallizes in the $ThMn_{12}$ tetragonal structure with space group $I4/mmm$. In this structure, the iron atoms occupy three inequivalent crystallographic sites, the 8f, 8i, and 8j sites, and the terbium occupies the 2a site. The titanium atoms are found only on the 8i site, the largest of the three iron sites. Neutron diffraction studies [8, 24, 25] indicate that the hydrogen is inserted only into the 2b site, an octahedral site with two terbium and four 8j iron near neighbours. Consequently, the maximum hydrogen uptake per formula unit is one. Gravimetric analysis of $TbFe_{11}TiH$ indicates that the maximum hydrogen uptake has been achieved and that the estimated hydrogen content is 1 ± 0.1 hydrogen atom/fu.

The lattice parameters and the unit-cell volume of $TbFe_{11}Ti$ and $TbFe_{11}TiH$ are given in table 1 and are in agreement with those previously reported [15]. Hydrogen insertion induces a small but significant unit cell increase of 3.7 Å^3 equivalent to 1.8 Å^3 per inserted hydrogen atom as the unit cell contains two molecules. This increase is anisotropic and occurs mainly in the (a, b) basal plane as is shown by the c/a ratio given in table 1.

The insertion of hydrogen into $TbFe_{11}Ti$ to form $TbFe_{11}TiH$ produces a significant increase in the Curie temperature from 578 to 620 K. In an earlier study [15], a slightly smaller increase from 560 to 595 K has been reported, a smaller increase which indicates that either the hydrogen uptake was smaller or the titanium content was different in the earlier sample. Similar increases in Curie temperature have been reported [3, 7, 26–28] for several isotypic compounds. These

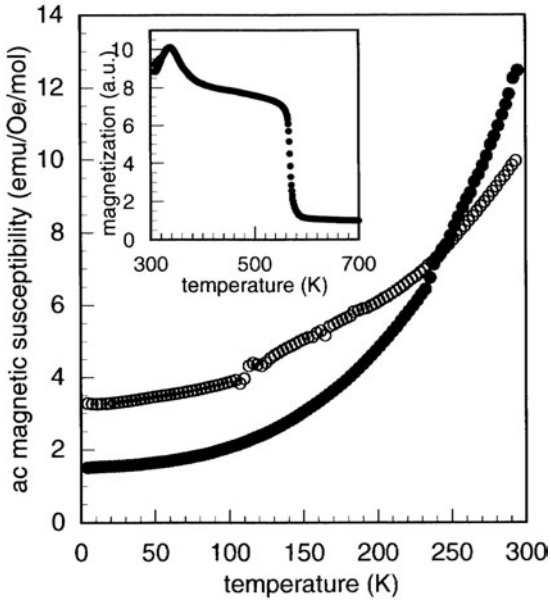

Figure 1. The temperature dependence of the ac magnetic susceptibility for $TbFe_{11}Ti$, closed symbols, and $TbFe_{11}TiH$, open symbols. The typical error bars are the size of the data points. Inset: the temperature dependence of the magnetization of $TbFe_{11}Ti$.

increases are related to the increase in the iron–iron interatomic distances and the concomitant increase in the 3d–3d magnetic exchange interactions.

The isothermal magnetization curves reveal that the insertion of hydrogen into $TbFe_{11}Ti$ increases the 5 K saturation magnetization from 10.5 to 11.3 μ_B/fu, and the 300 K values from about 11.7 to 12.2 μ_B/fu. The saturation magnetization is larger at 300 K than at 5 K because the terbium contribution to the magnetization is opposed to the iron contribution and decreases rapidly with increasing temperature.

The peak in the temperature dependence of the $TbFe_{11}Ti$ magnetization, see the inset to figure 1, yields a spin-reorientation temperature of 338 K, a value which is in good agreement with earlier studies [17]. Thus, the easy magnetization direction changes from parallel to the *c*-axis above 338 K to some direction within the basal plane below 338 K. This spin reorientation occurs because the iron sublattices favour a uniaxial magnetic anisotropy parallel to the *c*-axis, whereas, because of terbium's negative second-order Stevens coefficient, α_J, the terbium sublattice favours a basal anisotropy. As a consequence, above 338 K the iron sublattice anisotropy dominates whereas, below 338 K, the terbium sublattice anisotropy dominates.

The ac magnetic susceptibility is known [14, 29] to be very sensitive to changes in the magnetization direction in rare-earth transition-metal intermetallic compounds. As is shown in figure 1, neither $TbFe_{11}Ti$ nor $TbFe_{11}TiH$ show any anomaly in their ac susceptibility between 4.2 and 300 K. Thus neither compound exhibits a spin reorientation between 4.2 and 300 K.

The temperature dependence of the $TbFe_{11}TiH$ magnetization exhibits no anomaly, and thus no spin reorientation, between 300 K and its Curie temperature of 620 K. The disappearance of the spin reorientation upon hydrogenation of $TbFe_{11}Ti$ to form $TbFe_{11}TiH$ indicates that the interstitial hydrogen reinforces the terbium sublattice magnetic anisotropy, such that the hydride shows basal magnetic anisotropy up to the Curie temperature, as has also been observed [30] upon hydrogenation of $DyFe_{11}Ti$. The dominance of the rare-earth

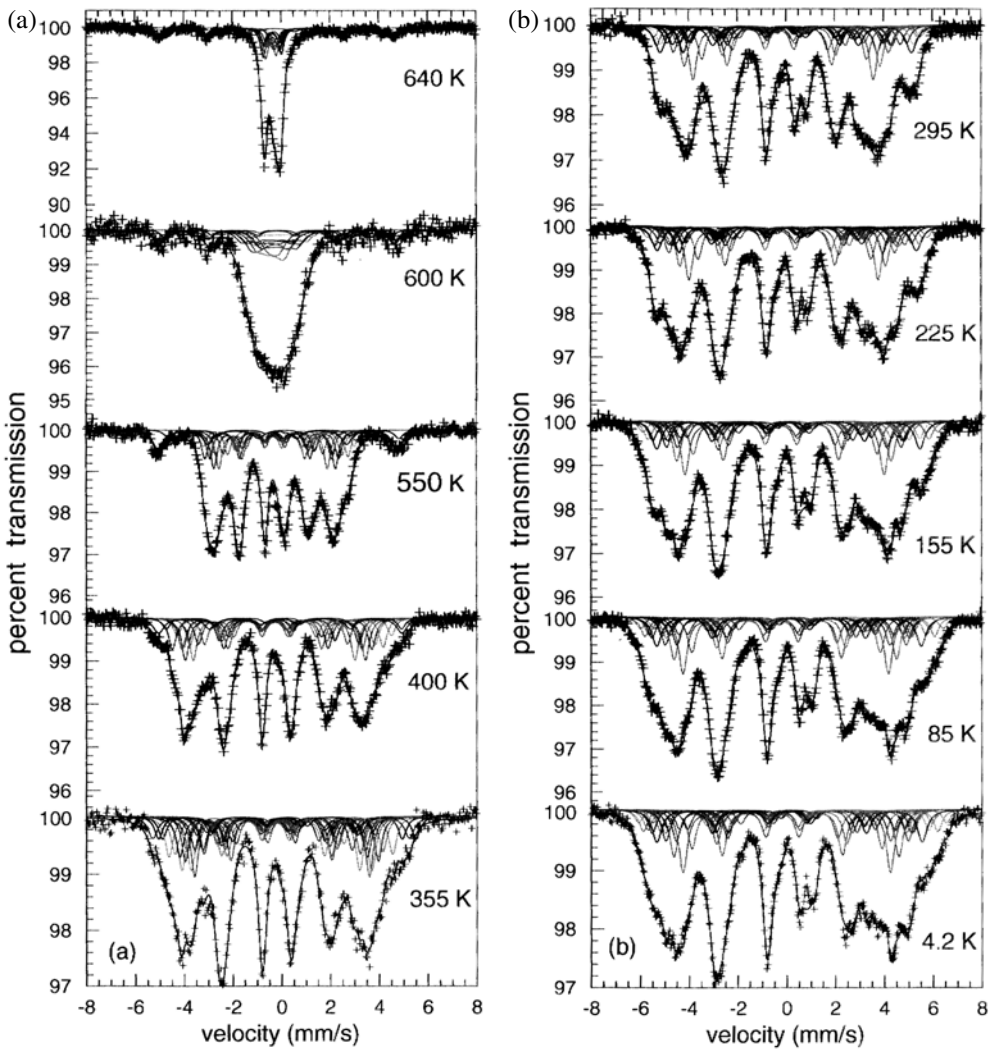

Figure 2. The Mössbauer spectra of $TbFe_{11}Ti$ obtained between 355 and 640 K (a) and 4.2 and 295 K (b).

magnetic anisotropy results from a relative increase in the crystalline electric field gradient at the rare-earth site in the presence of hydrogen.

4. Mössbauer spectral measurements

The Mössbauer spectra of $TbFe_{11}Ti$, obtained between 4.2 and 650 K, are shown in figures 2(a) and (b). The spectra at 550, 600, and 640 K clearly reveal the presence of two impurity phases. One of the impurity sextets is α-iron and has a relative area of 5%. The second sextet, with a slightly smaller hyperfine field and a relative area of 3%, cannot be assigned to Tb_2Fe_{17} which is paramagnetic at about 400 K. We tentatively assign this sextet to an iron–titanium alloy. However, this second impurity was not detected in the x-ray diffraction pattern. Alternatively, both contributions can be fit with a sextet with hyperfine parameters constrained to the known

hyperfine parameters for α-iron but with a relatively large line width of about 0.45 mm s^{-1}. This alternative fitting model is used herein for the spectra of $TbFe_{11}Ti$.

All the Mössbauer spectra of $TbFe_{11}Ti$ obtained between 4.2 and 295 K (figure 2(b)) have the same overall shape and correspond to a magnetic phase in which the easy magnetization direction, and hence the iron magnetic moments, are aligned in the basal plane of the tetragonal unit cell. The spectra of $TbFe_{11}Ti$ obtained between 355 and 550 K (figure 2(a)) have a different shape and correspond to a magnetic phase in which the easy magnetization direction, and hence the iron magnetic moments, are aligned along the *c*-axis of the tetragonal unit cell. This change in the Mössbauer spectral shape between 295 and 355 K agrees with the reported spin-reorientation temperature of 338 K. The Mössbauer spectra shown in figure 2(a) indicate that $TbFe_{11}Ti$ still exhibits long-range magnetic ordering at 600 K and becomes fully paramagnetic at 640 K. The small magnetic contribution to the spectrum at 640 K is due to the α-iron impurity. Hence, the Mössbauer spectra indicate a Curie temperature of 620 ± 20 K, a temperature which is significantly higher than that of 578 K determined from the magnetization measurements; see section 3. This difference is likely to result from the extrapolation used to obtain the Curie temperature from the magnetization measurements.

The Mössbauer spectra of $TbFe_{11}TiH$ obtained between 4.2 and 295 K are shown in figure 3. They all exhibit the same overall shape, a similarity which confirms [12, 15] that the magnetic anisotropy of $TbFe_{11}TiH$ does not change with temperature, in agreement with the thermomagnetic analysis discussed above. A small amount, 7%, of α-iron impurity is observed and included in the fits of the spectra.

All the magnetic spectra shown in figures 2 and 3 have been fit with a model which takes into account both the distribution of the titanium atoms in the neighbourhood of the three (8f, 8i, and 8j) iron sites and the easy magnetization direction. This model has already been successfully applied [30–33] to fit the Mössbauer spectra of the $RFe_{11}Ti$ compounds and their hydrides when R is Gd, Dy, Er, and Ho. The random occupation of the 8i sites by titanium results into a binomial distribution of the titanium near neighbours of the three iron sites. Hence, the 8i sextet is subdivided into three sextets with 6.47%, 10.79%, and 9.98% areas, and each of the 8f and 8j sextets is subdivided into three sextets with 11.51%, 15.34%, and 9.52% areas, sextets which represent the iron with zero, one, and two or more titanium near neighbours, respectively. Hence, at least nine sextets, with their areas fixed to the above relative values, are required to accurately model the Mössbauer spectra of $TbFe_{11}Ti$ above its spin-reorientation temperature in the uniaxial magnetic phase.

In the basal magnetic anisotropy phases of $TbFe_{11}Ti$ and $TbFe_{11}TiH$, a further subdivision of the three sextets assigned to each inequivalent iron site may be necessary. Because of the alignment of the iron magnetic moments, and consequently of the hyperfine fields, in the basal plane, multiple relative orientations of the principal axis of the electric field gradient, V_{zz}, and the hyperfine field occur and yield different angles, θ, between these two directions; the different directions yield different quadrupole shifts and slightly different hyperfine fields.

A close examination of the symmetry at the three iron sites in the $ThMn_{12}$ structure indicates that for one half of the 8i and 8j sites V_{zz} is along the [100] direction and for the other half V_{zz} is along the [010] direction. For one half of the 8f sites, V_{zz} is along the [110] direction and for the other half V_{zz} is along the $[1\bar{1}0]$ direction. If the compound exhibits a uniaxial magnetic anisotropy, i.e., the easy magnetization direction is along the crystallographic *c*-axis, then $\theta = 90°$ for the 8f, 8i, and 8j sites and no additional splitting of the nine spectral components described above is required. However, the situation changes when the easy magnetization direction is not parallel to the *c*-axis. In the $RFe_{12-x}M_x$ compounds, when the magnetization lies in the basal plane, two different alignments of the magnetic moments are possible, i.e., the moments may be parallel to the [110] or $[1\bar{1}0]$ directions or parallel to the

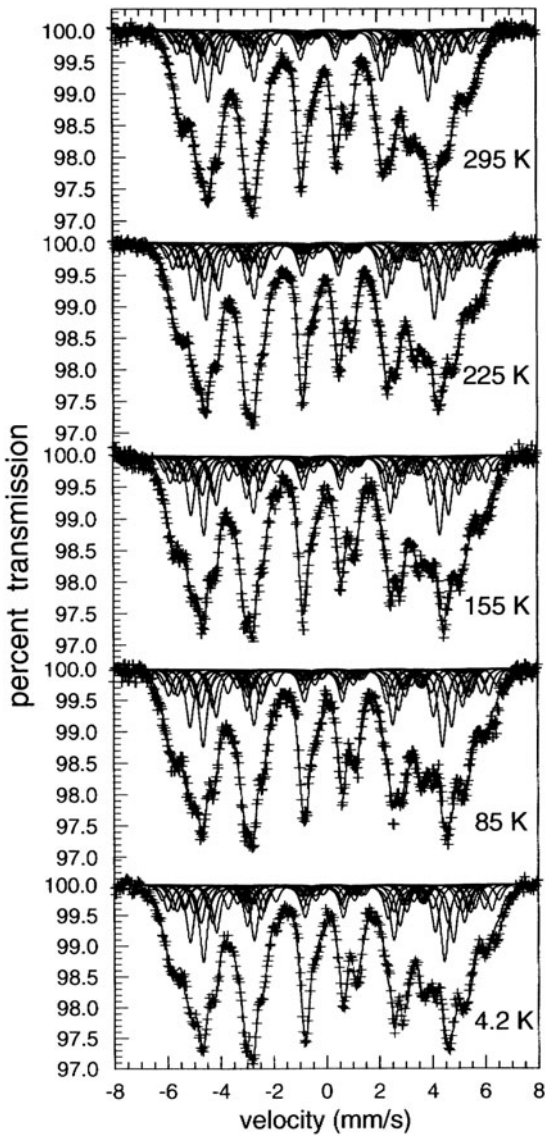

Figure 3. The Mössbauer spectra of $TbFe_{11}TiH$ obtained between 4.2 and 295 K.

[100] or [010] directions. In the first case, if the iron magnetic moments are aligned along the [110] or [1$\bar{1}$0] directions, there is no further magnetic subdivision of the sextets representing the 8i and 8j sites for which θ equals 45°. In contrast, there is a further magnetic subdivision of the sextets representing the 8f sites, into two groups of equal relative area, one with $\theta = 0°$ and one with $\theta = 90°$. Hence, each sextet assigned to the 8f site should be subdivided into two sextets of equal relative areas with identical isomer shift but different quadrupole shifts and slightly different hyperfine fields. As a consequence the Mössbauer spectra should be fit with 12 sextets. In the second case, if the iron magnetic moments are aligned along the [100] or [010] directions, there is no further magnetic subdivision of the sextets representing the 8f site for which θ equals 45°. In contrast, there is a further magnetic subdivision of those sextets

representing the 8i and 8j sites into two groups of equal relative area, one with $\theta = 0°$ and one with $\theta = 90°$. Hence, each sextet assigned to the 8i and 8j sites should be subdivided into two sextets of equal relative areas with identical isomer shift but different quadrupole shifts and slightly different hyperfine fields, and the Mössbauer spectra should be fit with 15 sextets.

The adequacy of both models, i.e., models with 12 and 15 sextets, in fitting the Mössbauer spectra of $TbFe_{11}Ti$ the $TbFe_{11}TiH$ between 4.2 and 295 K has been evaluated and the fits obtained with 12 sextets have been judged to be significantly poorer, with a misfit parameter of 0.6%, than those obtained with 15 sextets, with a misfit parameter of 0.2%. Further, the 12-sextet fits gave a very large and unrealistic line width of 0.50 mm s^{-1} for each sextet. Consequently, we preferred the 15-sextet fits even though this model contains more parameters. Thus we conclude that the Mössbauer spectra between 4.2 and 295 K are most compatible with the iron magnetic moments aligned along the [100] or [010] directions.

Three hyperfine parameters define each sextet, the hyperfine field, H, the isomer shift, δ, and the quadrupole shift, ε. In order to both build constraints into the model and to reduce the number of adjustable parameters, we assume that the three hyperfine parameters for each crystallographically inequivalent iron site vary linearly with the number, n, of titanium near neighbours, as given by

$$H_n = H_0 + n\Delta H,$$
$$\delta_n = \delta_0 + n\Delta\delta,$$

and

$$\varepsilon_n = \varepsilon_0 + n\Delta\varepsilon,$$

where H_0, δ_0, and ε_0 are the hyperfine field, isomer shift, and quadrupole shift, respectively, for zero titanium near neighbours and ΔH, $\Delta\delta$, and $\Delta\varepsilon$, are the changes in the hyperfine field, isomer shift, and quadrupole shift, respectively, for one additional titanium near neighbour. A similar linear dependence of the hyperfine field on the number of substitutional near-neighbour atoms has been successfully used [34–37] in the analysis of the Mössbauer spectra of the $R_2Fe_{17-x}M_x$ solid solutions. Hence, between 355 and 550 K, the Mössbauer spectra of $TbFe_{11}Ti$ have been fit with nine sextets, which involve 18 hyperfine parameters, one line width, and one total absorption area. All the remaining magnetic spectra shown in figures 2 and 3 have been fit with 15 sextets with 26 hyperfine parameters, one line width, and one total absorption area. All the fits are very good and their hyperfine parameters are given in tables 2 and 3.

The 640 K paramagnetic Mössbauer spectrum of $TbFe_{11}Ti$ has been fit using a spectral distribution similar to that used in the axial magnetic phase. Specifically, the spectrum has been fit with nine symmetric doublets, with relative areas fixed to the values used for the nine sextets between 355 and 550 K. Further, the two relevant hyperfine parameters, the isomer shift and quadrupole splitting, for each inequivalent crystallographic site, were forced to vary linearly with n, the number of titanium near neighbours. It is obvious that the fit of the 640 K spectrum, whose hyperfine parameters are given in table 2, is far from unique. Consequently, as is discussed in section 5, several constraints have been used to select this fit.

Because of the number of parameters mentioned above, it would seem likely that it should be easy to obtain several equally different good fits but that the fits would be far from unique. Hence, in the next section we discuss the temperature dependences of the hyperfine parameters and their relations with the crystallographic structure and indicate how they give confidence to the spectral analysis, its physical meaning, and the extent to which the fits are unique. Our past experience indicates that it is not as easy as might be anticipated to find good fits of the observed spectra especially when physically viable variations in the hyperfine

Table 2. Mössbauer spectral hyperfine parameters for $TbFe_{11}Ti$.

Parameter	T (K)	8f	$8i_1$	$8i_2$	$8j_1$	$8j_2$	Wt. Av.
$H_0(\Delta H)$	640	0.0	0.0	—	0.0	—	0.0
(T)	600	5.5(−1.8)	8.2(−1.3)	—	7.4(−1.6)	—	5.4
	400	22.9(−2.4)	27.3(−1.9)	—	25.4(−2.5)	—	22.8
	355	23.9(−2.1)	30.6(−2.0)	—	26.6(−2.4)	—	24.4
	295	24.9(−1.9)	34.0(−1.7)	32.1(−3.2)	30.0(−2.0)	27.0(−2.3)	26.2
	225	26.2(−2.1)	35.6(−1.8)	33.1(−3.1)	30.8(−2.1)	28.9(−3.0)	27.4
	155	27.3(−1.9)	37.6(−1.8)	34.1(−3.1)	32.0(−2.1)	29.8(−3.2)	28.6
	85	28.3(−2.2)	38.5(−1.6)	35.1(−3.3)	32.8(−2.1)	30.3(−3.2)	29.4
	4.2	28.6(−2.3)	39.2(−1.7)	35.5(−3.3)	33.0(−2.2)	30.6(−3.3)	29.7
δ_0[a] $(\Delta\delta)$	640	−0.450(0.050)	−0.161(−0.025)	—	−0.390(0.044)	—	−0.325
(mm s^{-1})	600	−0.410(0.050)	−0.134(−0.025)	—	−0.368(0.043)	—	−0.295
	550	−0.373(0.051)	−0.107(−0.026)	—	−0.334(0.043)	—	−0.262
	400	−0.330(0.044)	−0.003(−0.032)	—	−0.285(0.048)	—	−0.203
	355	−0.289(0.040)	0.055(−0.030)	—	−0.250(0.046)	—	−0.161
	295	−0.220(0.032)	0.126(−0.030)	0.126(−0.030)	−0.207(0.054)	−0.207(0.054)	−0.101
	225	−0.190(0.031)	0.166(−0.039)	0.166(−0.039)	−0.170(0.052)	−0.170(0.052)	−0.069
	155	−0.160(0.023)	0.187(−0.038)	0.187(−0.038)	−0.120(0.052)	−0.120(0.052)	−0.037
	85	−0.126(0.019)	0.214(−0.038)	0.214(−0.038)	−0.075(0.054)	−0.075(0.054)	−0.001
	4.2	−0.104(0.019)	0.224(−0.034)	0.224(−0.034)	−0.047(0.057)	−0.047(0.057)	0.022
ε_0 $(\Delta\varepsilon)$	640[b]	−0.220(0.003)	0.135(0.015)	—	−0.371(0.002)	—	−0.172
(mm s^{-1})	600	−0.080(0.076)	0.118(0.028)	—	−0.184(0.108)	—	0.008
	550	−0.080(0.076)	0.118(0.028)	—	−0.184(0.108)	—	0.008
	400	−0.112(0.081)	0.025(0.080)	—	−0.206(0.178)	—	0.005
	355	−0.097(0.088)	−0.056(0.171)	—	−0.188(0.196)	—	0.031
	295	0.121(0.025)	−0.146(0.050)	0.230(−0.295)	−0.528(0.157)	0.300(−0.157)	−0.025
	225	0.133(0.009)	−0.183(0.012)	0.223(−0.295)	−0.478(0.157)	0.330(−0.157)	−0.040
	155	0.145(−0.004)	−0.001(−0.100)	0.140(−0.295)	−0.385(0.157)	0.135(−0.157)	−0.046
	85	0.164(−0.008)	−0.060(−0.081)	0.001(−0.295)	−0.344(0.157)	0.062(−0.157)	−0.053
	4.2	0.182(−0.007)	−0.043(−0.110)	0.015(−0.295)	−0.288(0.157)	0.017(−0.157)	−0.055

[a] Relative to α-iron at room temperature.
[b] The paramagnetic quadrupole splitting.

parameters with temperature are imposed upon the fits. Indeed, we have not been able to find an alternative model that yields both good fits and viable variations in the hyperfine parameters with temperature; however, such an undiscovered model may, of course, exist.

5. Discussion

5.1. Hyperfine fields

The assignment and temperature dependence of the three hyperfine fields for zero titanium near neighbours and their weighted average for $TbFe_{11}Ti$ and $TbFe_{11}TiH$ are shown in figures 4(a) and (b), respectively. A Wigner–Seitz cell analysis [38] of the three inequivalent iron sites in $RFe_{11}Ti$ and $RFe_{11}TiH$ indicates that the 8i site has 11.75 iron near neighbours, the largest average number of iron near neighbours, whereas the 8f and 8j iron sites both have nine iron near neighbours. Consequently, the sextets with the largest hyperfine field, H_0, have been assigned to the 8i site, on the basis of both its percentage contribution to the spectral absorption area and its iron near-neighbour environment, an assignment that is further supported by the observed isomer shift values; see below. Because of both their identical constrained percentage spectral

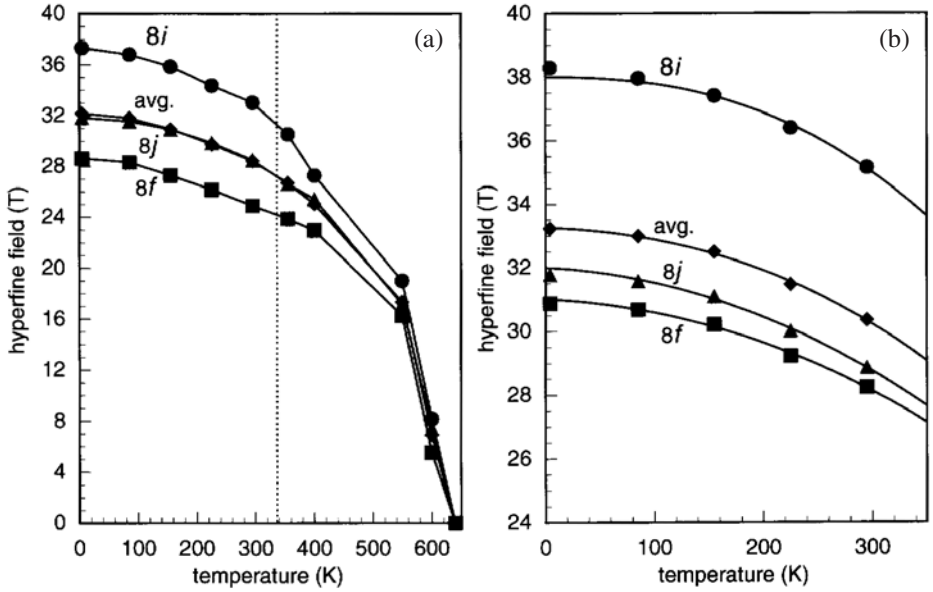

Figure 4. The Mössbauer dependence of the maximum hyperfine fields, H_0, at the three iron sites, and their weighted average, in $TbFe_{11}Ti$ (a) and $TbFe_{11}TiH$ (b). The dotted line indicates the spin-reorientation temperature.

Table 3. Mössbauer spectral hyperfine parameters for $TbFe_{11}TiH$.

Parameter	T (K)	8f	$8i_1$	$8i_2$	$8j_1$	$8j_2$	Wt. Av.
H_0 (ΔH)	295	28.2(−2.4)	36.0(−1.5)	34.3(−3.3)	29.0(−2.1)	28.7(−2.5)	27.9
(T)	225	29.2(−2.4)	37.6(−1.5)	35.2(−3.0)	30.2(−2.3)	29.8(−2.5)	29.1
	155	30.2(−2.5)	38.5(−1.5)	36.2(−3.1)	31.4(−2.6)	30.8(−2.5)	30.0
	85	30.7(−2.6)	39.0(−1.5)	36.8(−3.0)	31.8(−2.5)	31.3(−2.6)	30.5
	4.2	30.8(−2.6)	39.5(−1.5)	37.1(−2.9)	32.0(−2.5)	31.5(−2.6)	30.8
δ_0[a] ($\Delta\delta$)	295	−0.271(0.049)	0.060(−0.010)	0.060(−0.010)	−0.030(0.045)	−0.030(0.045)	−0.064
(mm s^{-1})	225	−0.212(0.047)	0.106(−0.010)	0.106(−0.010)	0.014(0.044)	0.014(0.044)	−0.015
	155	−0.176(0.047)	0.143(−0.012)	0.143(−0.012)	0.055(0.043)	0.055(0.043)	0.022
	85	−0.148(0.047)	0.160(−0.014)	0.160(−0.014)	0.080(0.041)	0.080(0.041)	0.045
	4.2	−0.138(0.047)	0.174(−0.014)	0.174(−0.014)	0.089(0.041)	0.089(0.041)	0.055
ε_0 ($\Delta\varepsilon$)	295	−0.053(0.051)	0.035(−0.121)	−0.103(−0.308)	0.338(0.169)	−0.004(−0.323)	−0.043
(mm s^{-1})	225	−0.057(0.051)	0.023(−0.074)	−0.157(−0.359)	0.360(0.241)	−0.029(−0.351)	−0.046
	155	−0.065(0.049)	0.027(−0.055)	−0.219(−0.337)	0.390(0.240)	0.004(−0.385)	−0.046
	85	−0.085(0.059)	−0.032(−0.037)	−0.172(−0.408)	0.393(0.262)	−0.031(−0.368)	−0.059
	4.2	−0.072(0.059)	−0.018(−0.037)	−0.193(−0.411)	0.399(0.263)	−0.041(−0.367)	−0.057

[a] Relative to α-iron at room temperature.

areas and their iron near-neighbour environments, it is not possible to unequivocally assign the 8f and 8j sextets on the basis of their fields, and their assignment is based on their isomer shifts; see below. Because the three H_0 hyperfine fields in $TbFe_{11}Ti$ increase upon hydrogenation as a consequence of lattice expansion, the sequence of hyperfine fields, 8i > 8j > 8f, remains unchanged; see figure 4(b). Further, a Wigner–Seitz cell analysis [38] indicates that, except for the 8j site which has one hydrogen in its near-neighbour environment, the near-neighbour environments of the 8f and 8i sites do not change upon hydrogenation.

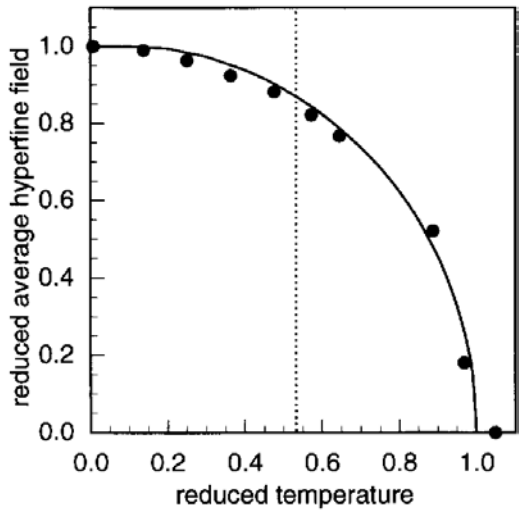

Figure 5. The reduced average hyperfine field versus the reduced temperature in $TbFe_{11}Ti$. The solid curve is the Brillouin curve for spin 5/2, and a Curie temperature of 620 K and a saturation field of 29.7 T have been used. The dotted line indicates the spin-reorientation temperature.

The solid curves in figure 4(b) are the result of a least-squares fit [39] with the equation

$$H = H_0[1 - B_{3/2}(T/T_C)^{3/2} - C_{5/2}(T/T_C)^{5/2}],$$

where H_0 and T_C are the saturation field and magnetic ordering temperature, respectively. The $T^{3/2}$ term in this equation has its origin [40] in the excitation of long-wavelength spin waves. The $B_{3/2}$ coefficients are about 0.01 and the $C_{5/2}$ coefficients are about 0.02, for all three sites and their weighted average.

A plot of the reduced average hyperfine field versus the reduced temperature in $TbFe_{11}Ti$ is shown in figure 5 together with a Brillouin function for spin 5/2. To obtain the reduced field, the 4.2 K average hyperfine field of 29.7 T was used and to obtain the reduced temperature an ordering temperature of 620 K as observed in the Mössbauer spectra was used. The agreement between the experimental points and the Brillouin function is good. There is no indication of a significant increase in the reduced hyperfine field at the spin reorientation in $TbFe_{11}Ti$. In contrast, an increase of hyperfine field with a uniaxial alignment has been observed in other rare-earth iron compounds [29, 37, 41–43], such as Tm_2Fe_{17}, $Pr_2Fe_{17}H_x$, and $Nd_6Fe_{13}Si$. The absence of a significant increase in hyperfine field for $TbFe_{11}Ti$ may result from the closeness of the spin-reorientation temperature and the Curie temperature.

In both $TbFe_{11}Ti$ and $TbFe_{11}TiH$ and in the other $RFe_{11}Ti$ compounds and their hydrides [3, 30–33], the 8i site exhibits the largest hyperfine field. This site results from the substitution of one rare-earth atom by two iron atoms within the $CaCu_5$ structure type, just as for the 6c site in the R_2Fe_{17} compounds, a site which also exhibits [29, 41, 44, 45] the largest hyperfine field in these compounds.

The hyperfine fields of the three iron sites in $TbFe_{11}TiH$ increase upon hydrogenation as a result of the observed lattice expansion. The changes in the hyperfine field per titanium near neighbour are between -1.5 and -3.4 T and are essentially independent of temperature in both $TbFe_{11}Ti$ and $TbFe_{11}TiH$. These observed decreases in the hyperfine fields upon the replacement of one iron by one titanium near neighbour are very similar to those observed [3, 30–33, 46] in the other $RFe_{11}Ti$ compounds and their hydrides, and are within the range of -1.1 to -6 T observed in a spinel oxide [47] and in $Nd_2Fe_{16}Ti$ [48], respectively.

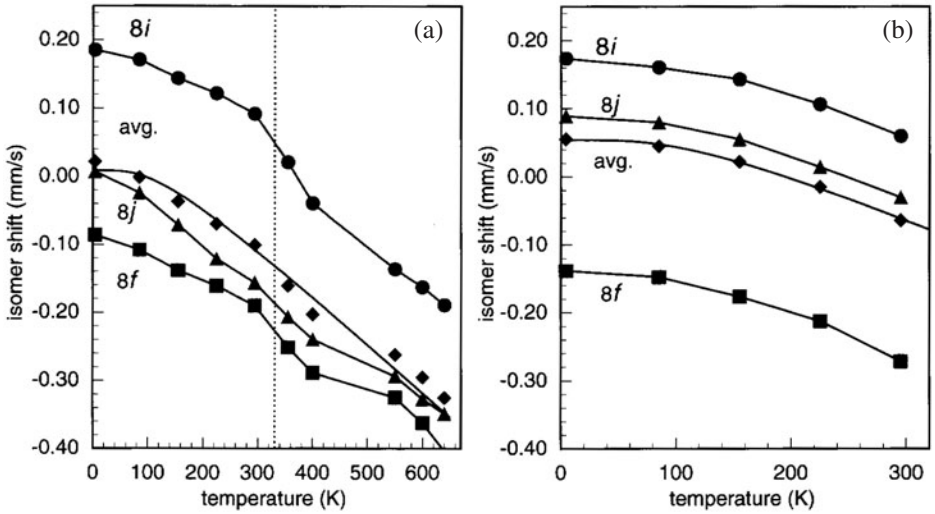

Figure 6. The temperature dependence of the three site average isomer shifts, and their weighted average, in $TbFe_{11}Ti$ (a) and $TbFe_{11}TiH$ (b). The dotted line indicates the spin-reorientation temperature.

5.2. Isomer shifts

The assignment and the temperature dependence of the three site average isomer shifts, and their weighted average, for $TbFe_{11}Ti$ and $TbFe_{11}TiH$ are shown in figures 6(a) and (b), respectively. The site average isomer shifts have been calculated from the δ_n-values weighted by the percentage contribution given by the binomial distribution. In agreement with the Wigner–Seitz cell analysis [38] of the three inequivalent iron sites, the sequence of isomer shifts, 8i > 8j > 8f, follows the sequence of Wigner–Seitz cell volumes. A similar correlation between the isomer shifts and the Wigner–Seitz cell volumes has been observed [29–33, 37, 41, 43, 44] in many $RFe_{11}Ti$, $R_6Fe_{13}X$, and R_2Fe_{17} compounds. The overall increase in unit-cell volume accounts for the increase in the weighted average isomer shift upon hydrogenation.

As is shown in figure 6(a), the isomer shifts observed for $TbFe_{11}Ti$ above the spin-reorientation temperature are somewhat lower than expected from the temperature dependence observed below the spin-reorientation temperature. Such a small decrease in isomer shifts at the spin reorientation has already been observed [29] in Tm_2Fe_{17} and was attributed to a small anisotropic magnetostriction accompanying the spin reorientation.

The temperature dependence of the weighted average isomer shifts shown in figures 6(a) and (b) has been fit [49, 50] with the Debye model for the second-order Doppler shift. For both compounds the resulting effective vibrating mass [50] is, as expected, 57 g mol^{-1} and the effective Mössbauer temperature is 456 ± 10 K. This temperature is typical of an intermetallic compound [29, 44, 51] and it would appear that the addition of the hydrogen has rather little influence on the Mössbauer temperature even though there is a 1% expansion of the lattice upon hydrogenation.

5.3. Quadrupole shifts and quadrupole splittings

The quadrupole shifts, ε, observed for the magnetic sextets and the quadrupole splittings, ΔE_Q, observed for the paramagnetic quadrupole doublets are related by the expression

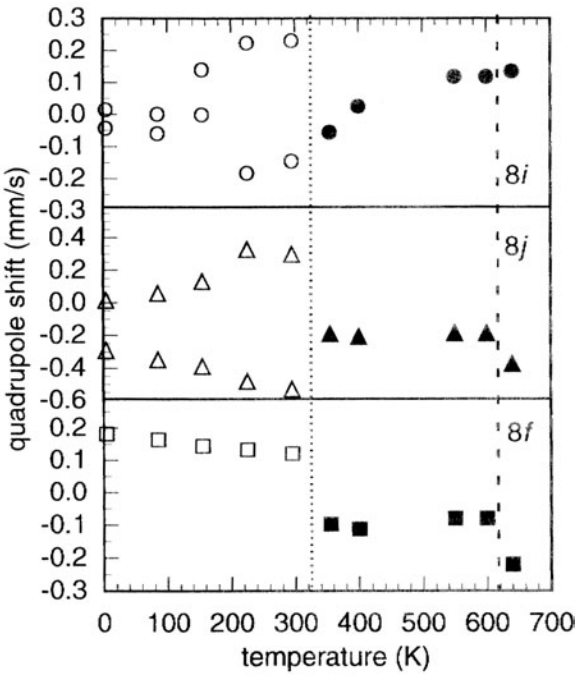

Figure 7. The temperature dependence of the zero titanium-neighbour quadrupole shifts, ε_0, and the quadrupole splitting, $\Delta E_{Q,0}$, at 640 K, for the three iron sites in $TbFe_{11}Ti$. The open and closed symbols are measured in the basal and axial magnetic phases, respectively. The dotted and dashed lines indicate the spin-reorientation and the Curie temperatures, respectively.

$\varepsilon = (1/2)\Delta E_Q(3\cos^2\theta - 1)$, where θ is the angle between the hyperfine field direction, which presumably is the easy magnetization direction, and the principal axis of the electric field gradient. Hence, in the case of $TbFe_{11}Ti$ an estimate of the θ-values can be obtained by comparing the quadrupole splittings measured at 640 K and the quadrupole shifts measured in both magnetic phases. This estimation will be done on the basis of the quadrupole shifts and splittings observed for the iron atoms with zero titanium atoms in their near-neighbour environment. The temperature dependence of the quadrupole shifts, ε_0, and the 640 K, quadrupole splittings, ΔE_{Q0}, for the three iron sites is shown in figure 7. In the basal magnetic phase between 4.2 and 295 K, there are two θ_0-values of 0° and 90° for both the 8i and 8j sites and one θ_0-value of 45° for the 8f site if, as discussed above, the hyperfine fields lie along the [100] or the [010] direction in the basal plane. As is shown in figure 7, the two ε_0-values for both the 8i and 8j sites differ in sign as expected for the $\theta = 0°$ and 90° values. However, the two values are not in the expected ratio of $-1/2$, perhaps because the error in the quadrupole shifts is rather large. In the magnetic axial phase, between 355 and 600 K, there is only one ε_0-value for each site, corresponding theoretically to $\theta = 90°$. If we use the above relationship between ε and ΔE_Q, measured at 550 and 640 K, we obtain θ-values of 60°, 90°, and 65° for the 8f, 8i, and 8j sites, respectively. By considering both the constraints introduced into the fitting model and the rather large error in the quadrupole shift values, these θ-values are very reasonable and, together with the temperature dependencies of the hyperfine fields and isomer shifts, support the Mössbauer spectral analysis.

6. Conclusions

From a macroscopic point of view the insertion of hydrogen into $TbFe_{11}Ti$ to form $TbFe_{11}TiH$ expands the lattice by 1%, increases the Curie temperature by 42 K, and increases the saturation magnetization by 0.8 and 0.5 μ_B/fu at 5 and 300 K, respectively. The combined ac magnetic susceptibility and thermomagnetic analysis shows the presence of a spin reorientation at 338 K in $TbFe_{11}Ti$. The planar terbium magnetic anisotropy dominates below 338 K, whereas the uniaxial iron magnetic anisotropy dominates above 338 K. In contrast, these measurements show no spin reorientations in $TbFe_{11}TiH$ below its Curie temperature of 640 K. Hence, hydrogen insertion modifies the balance between the terbium and iron sublattice magnetic anisotropies.

The Mössbauer spectral investigation confirms the magnetic measurements in establishing that in $TbFe_{11}Ti$ the iron magnetic moments are aligned along the *c*-axis and along the *a*-axis or *b*-axis of the structure above and below 338 K, respectively. In $TbFe_{11}TiH$ the refined hyperfine parameters are consistent with an alignment of the iron moments along the *a*-axis or *b*-axis between 4.2 and 295 K. Further, the temperature dependence of the magnetization shows the same alignment up to the Curie temperature. Hence the insertion of hydrogen into $TbFe_{11}Ti$ to form $TbFe_{11}TiH$ reinforces the terbium sublattice anisotropy.

From a microscopic point of view the insertion of hydrogen increases all three iron hyperfine fields, increases that are in agreement with the observed lattice expansion. Further, the insertion increases the average isomer shift, an increase that is in agreement with the changes in the Wigner–Seitz cell volume upon hydrogenation. The temperature dependence of the reduced hyperfine field in $TbFe_{11}Ti$ follows a Brillouin curve for spin 5/2.

Acknowledgments

The financial support of the University of Liège through grant number 2850006 is acknowledged with thanks. FG thanks the Fonds National de la Recherche Scientifique, Belgium, for grant number 9.456595. This work was partially supported by the US National Science Foundation through grants DMR95-21739 and INT-9815138, and the Centre National de la Recherche Scientifique, France, through grant action initiative number 7418.

References

[1] Buschow K H J 1994 *Electronic and Magnetic Properties of Metals and Ceramics* (*Materials Science and Technology Series* vol 3B) Part II, ed K H J Buschow (Berlin: VCH) p 451
[2] Hu B P, Li H S, Gavigan J P and Coey J M D 1989 *J. Phys.: Condens. Matter* **1** 755
[3] Long G J, Hautot D, Grandjean F, Isnard O and Miraglia S 1999 *J. Magn. Magn. Mater.* **202** 100
[4] Plugaru N, Rubin J, Bartolomé J, Piquer C and Artigas M 2002 *Phys. Rev.* B **65** 134419
[5] Buschow K H J 1997 *Handbook of Magnetic Materials* vol 10, ed K H J Buschow (Amsterdam: Elsevier) p 463
[6] Zhang L Y and Wallace W E 1989 *J. Less-Common Met.* **149** 371
[7] Isnard O, Guillot M, Miraglia S and Fruchart D 1996 *J. Appl. Phys.* **79** 5542
[8] Isnard O, Miraglia S, Guillot M and Fruchart D 1998 *J. Alloys Compounds* **275–277** 637
[9] Hurley D P F 1993 *PhD Thesis* Trinity College, Dublin
[10] Qi Q, Li Y P and Coey J M D 1992 *J. Phys.: Condens. Matter* **4** 8209
[11] Hurley D P F and Coey J M D 1992 *J. Phys.: Condens. Matter* **4** 5573
[12] Nikitin S A, Tereshina I S, Verbetsky V N, Salamova A A, Skokov K P, Pankratov N Yu, Skourski Yu V, Tristan N V, Zubenko V V and Telegina I V 2001 *J. Alloys Compounds* **322** 42
[13] Gu Z F, Zeng D C, Liu Z Y, Liang S Z, Klasse J C P, Brück E, de Boer F R and Buschow K H J 2001 *J. Alloys Compounds* **321** 40
[14] Kou X C, Zhao T S, Grössinger R, Kirchmayer H R, Li X and de Boer F R 1993 *Phys. Rev.* B **47** 3231
[15] Nikitin S A, Tereshina I S, Verbetsky V N and Salamova A A 2001 *J. Alloys Compounds* **316** 46

[16] Abadia C, Algarabel P A, Garcia-Landa B, Ibarra M R, del Morral A, Kudrevatykh N V and Markin P E 1998 *J. Phys.: Condens. Matter* **10** 349
[17] Boltich E B, Ma B M, Zhang L Y, Pourarian F, Malik S K, Sankar S G and Wallace W E 1989 *J. Magn. Magn. Mater.* **78** 364
[18] Guslienko K Yu, Kou X C and Grössinger R 1995 *J. Magn. Magn. Mater.* **150** 383
[19] Hu B P, Li H S and Coey J M D 1989 *Hyperfine Interact.* **45** 233
[20] Andreev A V, Kudrevatykh N V, Razgonyaev S M and Tarasov E N 1993 *Physica* B **183** 379
[21] Zhang L Y, Ma B M, Zhang Y and Wallace W E 1991 *J. Appl. Phys.* **70** 6119
[22] Barlet A, Genna J C and Lethuillier P 1991 *Cryogenics* **31** 801
[23] Rillo C, Lera F, Badia A, Angurel L, Bartolomé J, Palacio F, Navarro R and Duyneveldt A J 1992 *Susceptibility of Superconductors and Other Spin Systems* ed R A Hein, J L Francavilla and D H Liebenberg (New York: Plenum)
[24] Tomey E, Isnard O, Fagan A, Desmoulins C, Miraglia S, Soubeyroux J L and Fruchart D 1993 *J. Alloys Compounds* **191** 233
[25] Apostolov A, Bezdushnyi R, Stanev N, Damianova R, Fruchart D, Soubeyroux J L and Isnard O 1998 *J. Alloys Compounds* **265** 1
[26] Isnard O, Vulliet P, Sanchez J P and Fruchart D 1998 *J. Magn. Magn. Mater.* **189** 47
[27] Li Z W, Zhou X Z and Morrish A H 1993 *J. Phys.: Condens. Matter* **5** 3027
[28] Brouha M, Buschow K H J and Miedema A R 1974 *IEEE Trans. Magn.* **10** 182
[29] Grandjean F, Isnard O and Long G J 2002 *Phys. Rev.* B **65** 64429
[30] Piquer C, Isnard O, Grandjean F and Long G J 2003 *J. Magn. Magn. Mater.* **263** 235
[31] Piquer C, Hermann R P, Grandjean F, Long G J and Isnard O 2003 *J. Appl. Phys.* **93** 3414
[32] Piquer C, Isnard O, Grandjean F and Long G J 2003 *J. Magn. Magn. Mater.* **265** 156
[33] Piquer C, Grandjean F, Long G J and Isnard O 2003 *J. Alloys Compounds* **353** 33–41
[34] Long G J, Marasinghe G K, Mishra S, Pringle O A, Hu Z, Yelon W B, Middleton D P, Buschow K H J and Grandjean F 1994 *J. Appl. Phys.* **76** 5383
[35] Middleton D P, Mishra S R, Long G J, Pringle O A, Hu Z, Yelon W B, Grandjean F and Buschow K H J 1995 *J. Appl. Phys.* **78** 5568
[36] Mishra S R, Long G J, Pringle O A, Middleton D P, Hu Z, Yelon W B, Grandjean F and Buschow K H J 1996 *J. Appl. Phys.* **79** 3145
[37] Hautot D, Long G J, Ezekwenna P C, Grandjean F, Middleton D P and Buschow K H J 1998 *J. Appl. Phys.* **83** 6736
[38] Gelato L 1981 *J. Appl. Crystallogr.* **14** 141
[39] Ok H N, Baek K S and Kim C S 1981 *Phys. Rev.* B **24** 6600
[40] Herring C and Kittel C 1951 *Phys. Rev.* **81** 869
[41] Hautot D, Long G J, Grandjean F, Isnard O and Miraglia S 1999 *J. Appl. Phys.* **86** 2200
[42] Hautot D, Long G J, Grandjean F, de Groot C H and Buschow K H J 1998 *J. Appl. Phys.* **83** 1554
[43] Isnard O, Long G J, Hautot D, Buschow K H J and Grandjean F 2002 *J. Phys.: Condens. Matter* **14** 12391
[44] Hautot D, Long G J, Grandjean F and Isnard O 2000 *Phys. Rev.* B **62** 11731
[45] Isnard O and Fruchart D 1994 *J. Alloys Compounds* **205** 1
[46] Tereshina I S, Gaczynsku P, Rusakov V S, Drulis H, Nikitin S A, Suski W, Tristan N V and Palewski T 2001 *J. Phys.: Condens. Matter* **13** 8161
[47] Dormann J L 1980 *Rev. Phys. Appl.* **15** 1113
[48] Grandjean F, Ezekwenna P C, Long G J, Pringle O A, L'Héritier Ph, Ellouze M, Luo H P and Yelon W B 1998 *J. Appl. Phys.* **84** 1893
[49] Long G J, Hautot D, Grandjean F, Morelli D T and Meisner G P 1999 *Phys. Rev.* B **60** 7410
Long G J, Hautot D, Grandjean F, Morelli D T and Meisner G P 2000 *Phys. Rev.* B **62** 6829
[50] Herber R H 1984 *Chemical Mössbauer Spectroscopy* ed R H Herber (New York: Plenum) p 199
[51] Long G J, Isnard O and Grandjean F 2002 *J. Appl. Phys.* **91** 1423